

Development of a microfluidic device for cell concentration and blood cell-plasma separation

M. Sneha Maria^{1,2} · B. S. Kumar¹ · T. S. Chandra² · A. K. Sen¹

Published online: 13 November 2015
© Springer Science+Business Media New York 2015

Abstract This work presents design, fabrication and test of a microfluidic device which employs Fahraeus-Lindqvist and Zweifach-Fung effects for cell concentration and blood cell-plasma separation. The device design comprises a straight main channel with a series of branched channels placed symmetrically on both sides of the main channel. The design implements constrictions before each junction (branching point) in order to direct cells that would have migrated closer to the wall (naturally or after liquid extraction at a junction) towards the centre of the main channel. Theoretical and numerical analysis are performed for design of the microchannel network to ensure that a minimum flow rate ratio (of 2.5:1, main channel-to-side channels) is maintained at each junction and predict flow rate at the plasma outlet. The dimensions and location of the constrictions were determined using numerical simulations. The effect of presence of constrictions before the junctions was demonstrated by comparing the performances of the device with and without constrictions. To demonstrate the performance of the device, initial experiments were performed with polystyrene microbeads (10 and 15 μm size) and droplets. Finally, the device was used for concentration of HL60 cells and separation of plasma and cells in diluted blood samples. The cell concentration and blood-plasma purification efficiency was quantified using Haemocytometer and Fluorescence-Activated Cell Sorter (FACS). A seven-fold cell

concentration was obtained with HL60 cells and a purification efficiency of 70 % and plasma recovery of 80 % was observed for diluted (1:20) blood sample. FACS was used to identify cell lysis and the cell viability was checked using Trypan Blue test which showed that more than 99 % cells are alive indicating the suitability of the device for practical use. The proposed device has potential to be used as a sample preparation module in lab on chip based diagnostic platforms.

Keywords Microfluidics · Cell-plasma separation · Passive separation

1 Introduction

Complete analysis of blood could provide a myriad of information about the overall functioning of human body, since it performs the most vital functions such as maintenance of homeostasis, transportation of nutrients, oxygen and immune cells to various tissues and organs (Hou et al. 2011). Blood is a complex non-Newtonian fluid and comprises two components - cell components suspended in protein rich plasma component. The cells include the leukocytes or white blood cells (WBCs) (typical size 10–15 μm) which occupy 0.7 % of blood by volume, erythrocytes or red blood cells (RBCs) (typical size $8 \times 2 \mu\text{m}$) which comprise 45 % of blood and platelets (typical size 1–3 μm). Investigation of the physical properties of cells present in blood samples could indicate presence or progress of many cell-based diseases including cancer, sickle-cell, sepsis and malaria (Gossett et al. 2010). The plasma is clear and of straw colour and occupies 54.3 % of blood. Monitoring the relative proportions of plasma proteins and inorganic compounds, which change due to certain diseases, can be a very effective diagnostic tool. A critical review by Kersaudy-Kerhoas and Sollier (2013) enumerates the different

✉ A. K. Sen
ashis@iitm.ac.in

¹ Department of Mechanical Engineering, Indian Institute of Technology Madras, Chennai 600036, India

² Department of Biotechnology, Indian Institute of Technology Madras, Chennai 600036, India

analytes and biomarkers of interest present in blood plasma. Separation of blood cells from plasma is one of the important sample preparation steps that needs miniaturization to realize lab on chip diagnostic devices (Sen et al. 2011).

Despite substantial automation of various blood tests available, the sample preparation is still being done in a crude manner that can alter the results of the ensuing tests. Conventionally, flow cytometry, centrifugation and filtration are used to achieve this goal (Zhong et al. 2012), which are associated with a number of limitations in terms of cost, time, labour intensiveness and contamination due to cell damage incurred during the process. Further, the sheer bulkiness of these instruments deters their application in theranostics. Efforts to use an egg beater to separate plasma from blood at severely resource-limited settings voice the importance of scaling down this process (Wong et al. 2008). Primary diagnostic tests in healthcare could be made accessible and affordable when the overall system could be miniaturized and simple. Thus, development of a simple microfluidic blood plasma separation device is critical which could enable point-of-care diagnosis, miniaturization of bulk assays, low sample and reagent volume, gentle manipulation, parallel processing, increased portability, high accuracy, speed and affordability (Zhong et al. 2012).

Attempts have been made to develop sample preparation techniques that meet the above demands but adequate performance levels in terms of purification efficiency and plasma recovery have not been achieved yet (Kersaudy-Kerhoas and Sollier 2013). The various cell-plasma separation techniques reported in literature can be grouped into two categories: active separation (Yeo et al. 2006; Nakashima et al. 2010; Liao et al. 2013; Jiang et al. 2011; Lenhof et al. 2009; Xu et al. 1999; Furlani 2007; Nam et al. 2012) and passive separation (Crowley and Pizziconi 2005; VanDelinder and Groisman 2006; Aran et al. 2011; Moorthy and Beebe 2003; Li et al. 2012; Chung et al. 2012; Homsy et al. 2012; Yoon et al. 2006; Dimov et al. 2011; Zhang et al. 2012; Sun et al. 2012; Faivre et al. 2006; Davis et al. 2006; Jaggi et al. 2007; Choi and Park 2007; Mach and Di Carlo 2010; Blatter et al. 2004; Haeberle and Brenner 2006; Nivedita and Papautsky 2013; Yang et al. 2006; Fan et al. 2008; Kersaudy-Kerhoas et al. 2010a, b; Bhardwaj et al. 2011; Prabhakar et al. 2015; Tripathi et al. 2013). Active separation techniques employ external fields such as acoustic, electric and magnetic fields for cell-plasma separation. Although, such techniques provide high purification efficiency, they are associated with limitations in terms of low input flow rate and throughput since a longer residence time is required for the particles to experience the force field for separation. On the other hand, passive separation is simpler and utilize only hydrodynamic forces within the flow that may occur due to the geometric features of the device, namely sedimentation, microfiltration and cell deviation owing to obstacles and various lift forces acting on the cell (Kersaudy-

Kerhoas and Sollier 2013). Here, separation is based on the inherent mechanical properties of the particles, such as size, shape and deformability. Since there can be considerable damage to the cells due to the large magnitude of the forces acting on the cells in active separation, passive mode of separation is found to produce least damaging effects on the cells and also could have advantages including high throughput, cost-effectiveness in terms of fabrication, ease of operation, lower power budget and portability (Kersaudy-Kerhoas and Sollier 2013; Prabhakar et al. 2015; Tripathi et al. 2013). Table 1 provides a summary of studies from literature on plasma separation employing active and passive techniques and the corresponding efficiency in terms of purification and plasma recovery. An extensive review of various methods that have been developed for particle-liquid separation is reported elsewhere (Hou et al. 2011; Gossett et al. 2010; Kersaudy-Kerhoas and Sollier 2013; Pamme 2007; Sajeesh and Sen 2014; Toner and Irimia 2005; Bhagat et al. 2010; Kersaudy-Kerhoas et al. 2008; Lenhof and Laurell 2010).

Most of the passive separation techniques reported in literature are capable of providing good purification efficiency but the plasma recovery is always compromised. For example, filtration methods (Crowley and Pizziconi 2005; VanDelinder and Groisman 2006; Aran et al. 2011; Moorthy and Beebe 2003; Li et al. 2012; Chung et al. 2012; Homsy et al. 2012) are capable of delivering ~100 % purification efficiency but such methods give rise to clogging issues and the plasma recovery is often found to be only ~15 %. Sedimentation methods (Yoon et al. 2006; Dimov et al. 2011; Zhang et al. 2012; Sun et al. 2012) have limitations in terms of the amount of time required for the separation process to complete. Various passive separation techniques based on migration of cells due to special geometry of the channels have been developed (Faivre et al. 2006; Davis et al. 2006; Jaggi et al. 2007; Choi and Park 2007; Mach and Di Carlo 2010; Blatter et al. 2004; Haeberle and Brenner 2006; Nivedita and Papautsky 2013; Yang et al. 2006; Fan et al. 2008; Kersaudy-Kerhoas et al. 2010a, b; Bhardwaj et al. 2011; Prabhakar et al. 2015; Tripathi et al. 2013). Such techniques enable separation of particles in a continuous manner and also overcome the limitations of separation speed and fabrication complexity. Among these, separation techniques based on centrifugal effects have been found to provide highest purification efficiency (Blatter et al. 2004; Haeberle and Brenner 2006; Nivedita and Papautsky 2013). However, the plasma recovery is found to be below 40 %. The Deterministic Lateral Displacement (DLD) technique has the potential to achieve high purification efficiency and plasma recovery but it has limitations in terms of clogging and device fabrication yield and more importantly the need for three-stage separation (i.e., for WBCs first followed by RBCs and platelets) (Davis et al. 2006). Kersaudy-Kerhoas et al. (2010a) have reported a device based on the Zweifach-Fung effects

Table 1 Plasma separation techniques from literature showing purification efficiency and plasma recovery

Publication details	Technique employed	Sample	Operating condition	Device performance
Active method of separation				
(Yeo et al. 2006)	Electric tempest	Sheep's blood	0.94 kV rms Freq ~90KHz Time – 200 s	Haematocrit – 0.4 % Plasma – 0.003 %
(Nakashima et al. 2010)	Dielectrophoresis and capillary forces	Human blood	AC 10 V 1 MHz	Haematocrit – 4.4 % Purification efficiency – 97 % Plasma recovery – 6 %
(Liao et al. 2013)	Capillary dielectrophoresis	Human blood	20 V at 100KHz 30s	Haematocrit – 10–50 % Purification efficiency – 90 % Plasma recovery – N/A
(Jiang et al. 2011)	Electro-osmotic flow field	Human blood	5 min	Haematocrit – 6.7 % Purification efficiency – 100 % Plasma recovery – 26.6 %
(Lenshof et al. 2009)	Acoustophoresis	Human blood	80 µl/min	Haematocrit – Whole blood Purification efficiency – 100 % Plasma recovery – 12.5 %
Passive method of separation				
(Crowley and Pizziconi 2005)	Transverse flow micro-filters	Bovine blood	Plasma flux – 35–175 µm/s	Haematocrit – 40 % Purification efficiency – ~100 % Plasma recovery – 0.9 %
(VanDelinder and Groisman 2006)	Continuous cross-flow filtration	Human blood	0.65 µl/min	Haematocrit – 20 % Purification efficiency – N/A Plasma recovery – 8 % Hemolysis – 11 mg/dl
(Aran et al. 2011)	Cross-flow filtration through membrane	Human blood	10 µl/min	Haematocrit – 30 % Purification efficiency – ~100 % Plasma recovery – 15 %
(Moorthy and Beebe 2003)	<i>In situ</i> fabricated porous chip	Rabbit blood	10–20 µl/min	Haematocrit – 3.3–45 % Efficiency comparable to centrifuge
(Li et al. 2012)	Dead-end filtration with packed beads and capillary actuation	Sheep blood	0.02 µl/min	Haematocrit – Whole blood Purification efficiency – 100 % Plasma recovery – ~2 %
(Chung et al. 2012)	Dead-end filtration with membrane filters and magnetic actuation	Human blood	50 µl/min	Haematocrit – Whole blood Purification efficiency – 100 % Plasma recovery – 14 %
(Homsy et al. 2012)	Filtration (Commercial blood filter membrane)	Human blood	<10 min P- 40 mbar, 7 min	Haematocrit – Whole blood Purification efficiency – N/A Plasma recovery – 12 %
(Yoon et al. 2006)	Sedimentation with cross-flow filtration		0.1 µl/min	Haematocrit – Whole blood Purification efficiency – N/A Plasma recovery – 20 %
(Dimov et al. 2011)	Sedimentation in trenches	Human blood	0.83 µl/min	Haematocrit – Whole blood Purification efficiency – 100 % Plasma recovery – N/A
(Zhang et al. 2012)	Sedimentation with back-facing step	Human blood	15 µl/min	Haematocrit – 8 % Purification efficiency – 99 % Plasma recovery – 66 %
(Sun et al. 2012)	Sedimentation in a plug	Human blood	0.5 µl/min	Haematocrit – 8 % Purification efficiency – 100 % Plasma recovery – 60 %
(Favre et al. 2006)	Constriction	Human blood	3.3×10^{-3} ml/min	Haematocrit – 16 % Purification efficiency – 100 % Plasma recovery – 18 %
(Davis et al. 2006)	Deterministic Lateral Displacement	Human blood	1.0 µl/min	Haematocrit – Whole blood Purification efficiency – 100 % Plasma recovery – 100 %
(Jaggi et al. 2007)	High aspect ratio channels	Human blood	5.0 ml/min	Haematocrit – 4.5 % Purification efficiency – 90 % Plasma recovery – 2.5 %

Table 1 (continued)

Publication details	Technique employed	Sample	Operating condition	Device performance
(Choi and Park 2007)	Slanted obstacles	Human blood	4.0 μ l/min	Haematocrit – 10 % Purification efficiency – N/A Plasma recovery – 40 %
(Mach and Di Carlo 2010)	Pure inertial force (hydrodynamic lift force)	Human blood	8.0 ml/min	Haematocrit – 0.5 % Purification efficiency – 100 % Plasma recovery – N/A
(Wong et al. 2008)	Egg beater centrifuge	Human blood	Spinning – 1200 rpm, 8.0 min	Haematocrit – Whole blood Purification efficiency – Cell concentration in plasma 50000 cells/ml Plasma recovery – 58 %
(Blatter et al. 2004)	Bend structures	Human blood	1.2 ml/min	Haematocrit – 5 % Purification efficiency – 90 % Plasma recovery – 3 %
(Haeberle and Brenner 2006)	Rotating disk - Centrifugal effect	Human blood	Spinning speed – 40 Hz, 20 s	Haematocrit – Whole blood Purification efficiency – 100 % Plasma recovery – 40 %
(Zhong et al. 2012)	Curved channel FahraeusLindqvist Zweifach Fung effect	Human blood	3.0 μ l/min	Haematocrit – Whole blood Purification efficiency – N/A Plasma recovery – N/A
(Nivedita and Papautsky 2013)	Spiral inertial microfluidic device	Human blood	~1.0 ml/min	Haematocrit – 0.45 % Purification efficiency – ~100 % Plasma recovery – N/A
(Yang et al. 2006)	Bifurcation law	Defibrinated sheep blood	1.67×10^{-3} ml/min	Haematocrit - <25 % Purification efficiency – 100 % Plasma recovery – 19 %
(Fan et al. 2008)	Zweifach Fung effect	Human blood	Plasma flux \rightarrow ~0.1 mm/s	Haematocrit – Whole blood Purification efficiency – ~100 % Plasma recovery – 100 %
(Kersaudy-Kerhoas et al. 2010a)	T channels	Mussel blood Human blood	10 ml/hr 10 ml/hr	Purification efficiency - 76.3 % Haematocrit – 3 % Purification efficiency - 53 % Plasma recovery – 40 %
(Kersaudy-Kerhoas et al. 2010b)	Bifurcation law	Human blood	2,5,10 ml/hr	<i>20 μm wide plasma channel</i> Haematocrit – <10 % Purification efficiency – 95– 100 % Plasma recovery – 30 % Haematocrit – 34 % Purification efficiency – 32 % Plasma recovery – 30 % <i>10 μm wide plasma channel</i> Haematocrit – 9–45 % Purification efficiency – ~100 % Plasma recovery – 5 %
(Prabhakar et al. 2015)	Fahraeus effect Bifurcation law Cell-free region centrifugal action Constriction	Human blood	0.3–0.5 ml/min	Haematocrit – Whole blood Purification efficiency - 80 % Plasma recovery – N/A
(Tripathi et al. 2013)	Elevated T channel	Human blood	0.15 ml/min	Haematocrit – 45 % Purification efficiency – 67 % Plasma recovery – N/A

which provided a purification efficiency of ~96 % with mussel blood and ~60.8 % for human blood (3 % haematocrit). The plasma yield of the device was measured to be ~40 %. Kersaudy-Kerhoas et al. (2010b) reported an improved device with modifications in the channel design which offered

~100 % purification efficiency of ~1.8 % haematocrit in a 20 μ m plasma channel and 100 % purification efficiency with 35 % haematocrit in a 10 μ m plasma channel. However, the plasma yield was found to be only 30 % and 5 % with 20 μ m and 10 μ m plasma channels, respectively. This plasma

recovery is low and could limit applications of such a device for detection of analytes in plasma present at low concentrations.

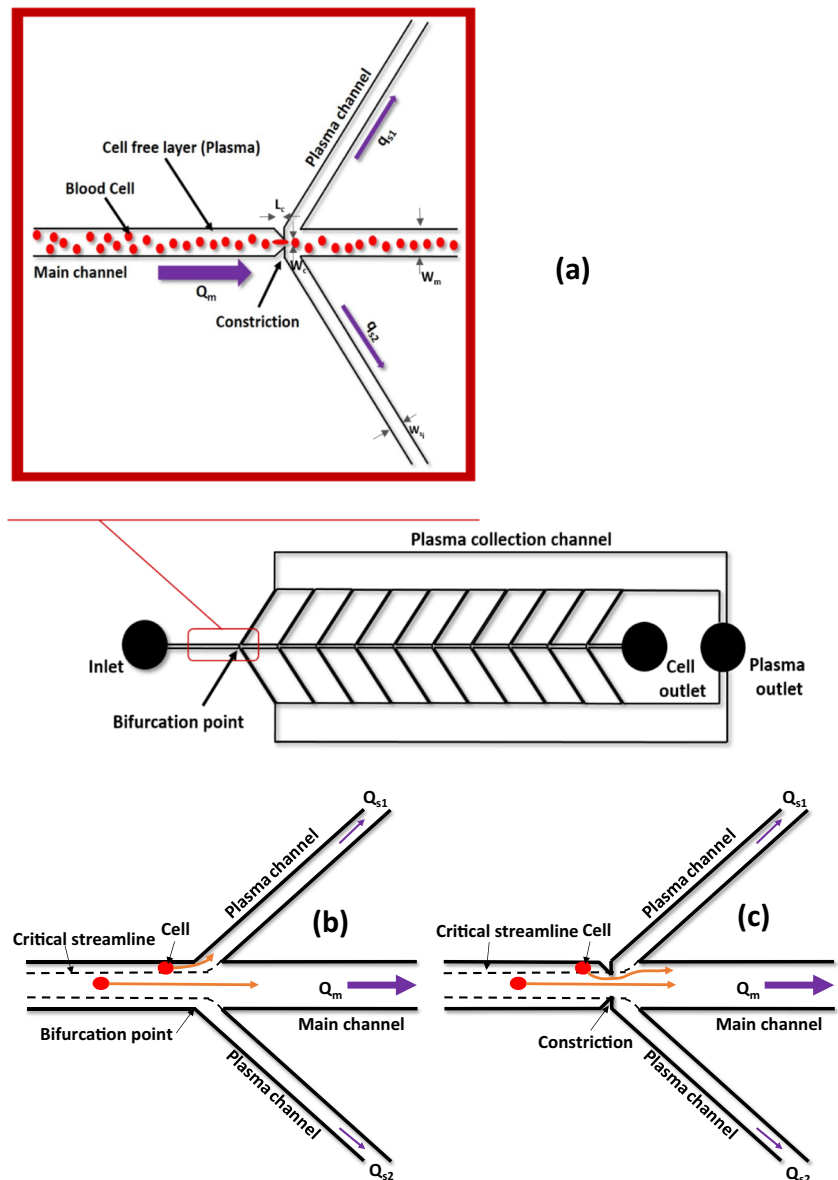
In this work, we present a blood-plasma separation device based on Fahraeus-Lindqvist (Narsimhan et al. 2013) and Zweifach-Fung (Yang et al. 2006) effects with a goal of achieving high plasma recovery along with good purification efficiency. The device also shows promise for use in cell concentration (e.g., concentration of pathogens in sample water). First, a detailed description of the device geometry and the operating principle are presented. Next, the theoretical approach and a numerical model are outlined which are used for design of the microchannel network and overall device geometry. Further, the experimental details including device fabrication, materials and methods and the experimental setup

and procedure are detailed. Then, the results of the theoretical analysis, numerical simulations and experiments with microbeads, droplets, HL60 cells and blood sample are presented and discussed.

2 Device description and principle

A schematic of the proposed microfluidic device for blood cell-plasma separation is depicted in Fig. 1a. The device comprises a straight main channel with a series of branched channels placed symmetrically on both sides of the main channel at equal interdistance. The branched channels on both sides of the main channel open into two wider channels which connect at the plasma outlet. The blood sample is infused into the

Fig. 1 a Schematic of the microfluidic device used for blood cell-plasma separation, illustration of a bifurcation and the role of constriction showing **b** the flow path of a cell at the centre of the channel and a cell below the critical streamline **c** the role of constriction in focusing the cell below the critical streamline to the centre of the channel



device through the inlet. When blood flows through microchannels, two important effects are observed, namely Fahraeus effect and Fahraeus-Lindqvist effect. Fahraeus effect states that the tube haematocrit is lesser than the feed haematocrit. This leads to Fahraeus Lindqvist effect, which states that the apparent viscosity of blood flowing through a tube (<300 μm) decreases with decrease in diameter. These strongly correlated effects occurs due to the formation of cell free layer by axial migration of cells towards the centre in a microchannel (Tripathi et al. 2015b).

Studies showing the disproportionate distribution of RBCs at bifurcation indicate that when the resistance in one of the bifurcating channel is increased, the entry of RBC into that channel can be prevented (Tripathi et al. 2015a). Thus, according to Zweifach-Fung effect, at a junction, the cells have a tendency to flow into the high flow rate branch provided a flow rate ratio of at least 2.5 is maintained (Yang et al. 2006). This can be taken care of by appropriate design of the microchannel network, as demonstrated by (Tripathi et al. 2015a), where the effects of geometrical parameters on the performance of microfluidic devices for plasma separation have been studied. In the proposed design, a minimum main channel to side channel flow rate ratio of 2.5 is maintained so the cells continue to move along the main channel and are collected at the cell outlet. The plasma is extracted through the branched side channels and collected at the plasma outlet. Although most of the cells would tend to migrate towards the centre of the main channel (due to Fahraeus-Lindqvist effect), particularly at high concentrations, some cells might be moving closer to the walls. Also, a recent work by Doyeux et al. (2011) concludes that in a network of bifurcations, the initially centred particles will migrate towards the wall after first bifurcation. However, such cells will be located only at a distance of the order of half the cell size from the channel walls. It is known that a particle present in a laminar flow move along a streamline passing through its centre of mass (Yamada et al. 2004). So there is a chance that such cells could move into the plasma channels thus affecting the purification efficiency. The device could be designed such that the streamlines passing through its centre of mass of cells do not enter the side branch channels and stay in the main channel. But such small dimensions of side channels could severely limit the plasma recovery. Also, this would provide a very high flow rate ratio which may lead to cell damage (Tripathi et al. 2013). Here, we introduce constrictions immediately before each junction to ensure that such cells are positioned at the centre at the junction and continue to move only along the main channel while the plasma is extracted through the side channels. The role of the constriction immediately before each junction is illustrated in Fig. 1b and c. The width of the main channel, W_m is 100 μm and the width of the side branch channels, W_s varies from 25 to 43 μm . The side branch channels are placed at an angle 130° with the main channel. The wider channels are of

250 μm width (W_c). The constriction is located just before the junction and the throat width of the constriction is 40 μm . The channel height h is 50 μm uniform throughout the fluidic network.

The proposed device differs from the design reported by Kersaudy-Kerhoas et al. (2010a) in that the dimensions of the side channels have been optimized to achieve moderate flow rate ratios at each of the junctions (4 to 7), which is critical for cell viability (Tripathi et al. 2013). Also, in our design, constrictions are introduced in front of every junction to facilitate alignment of the cells towards the centre, to improve the separation efficiency (section 6.4). Additionally, the proposed device offers higher plasma recovery as compared to the device reported by Kersaudy-Kerhoas et al. (2010a) (section 6.4).

3 Theoretical model

The entire fluidic network was analysed to predict the flow rate ratio (main-to-side branch channels) at each junction and the total flow rate at the plasma outlet. First, the fluidic network is converted to an equivalent electrical network with the hydrodynamic resistance R defined as $R = \Delta P/Q$, where ΔP is the pressure drop and Q is the flow rate, which are related as follows,

$$Q = \frac{h^4 \Delta P}{12 \mu L \alpha} \left[1 - \sum_{n=1,3,5}^{\infty} \frac{192 \alpha}{(n\pi)^5} \tanh\left(\frac{n\pi}{2\alpha}\right) \right] \quad (1)$$

Where $\alpha = h/w$ is the aspect ratio of the channel, w is the width of the channel of length L . A schematic of a part of the fluidic network with only first two junctions and its equivalent resistance network are depicted in Fig. 2a and b. Here, R_{m0} is the resistance of the channel from the inlet to the first junction, R_{sm1} are the resistances of the first two side branch channels (which are equal) and R_{s1} is the resistance of the wider channels between first two branches and R_{m1} is the resistance of the channel between first and second bifurcations. Similarly, R_{sm2} , R_{s2} and R_{m2} can be defined at the second junction. Using analogy between the hydrodynamic and electrical circuits for this section of the channel, if the hydrodynamic resistances are directly used as electrical resistances, the pressure drop $\Delta P_{1,2}$ across the channel can be replaced by equivalent voltage drop $V_{1,2}$ and flow rate by current $I_{1,2}$. Such an equivalent electrical circuit is depicted in Fig. 2c. Now, if we apply Kirchoff's law for this circuit,

$$V_{1,2} - I_{1,2}R_{m0} - (I_{1,2} - I_2)R_{m1} - (I_{1,2} - I_3)R_{m2} = 0 \quad (2)$$

$$-\left(\frac{R_{sm1}}{2} + \frac{R_{s1}}{2}\right)I_2 - \frac{R_{sm2}}{2}(I_2 - I_3) - R_{m1}(I_2 - I_{1,2}) = 0 \quad (3)$$

$$-\frac{R_{sm2}}{2}(I_3 - I_2) - \frac{R_{s2}}{2}(I_3) - R_{m2}(I_3 - I_{1,2}) = 0 \quad (4)$$

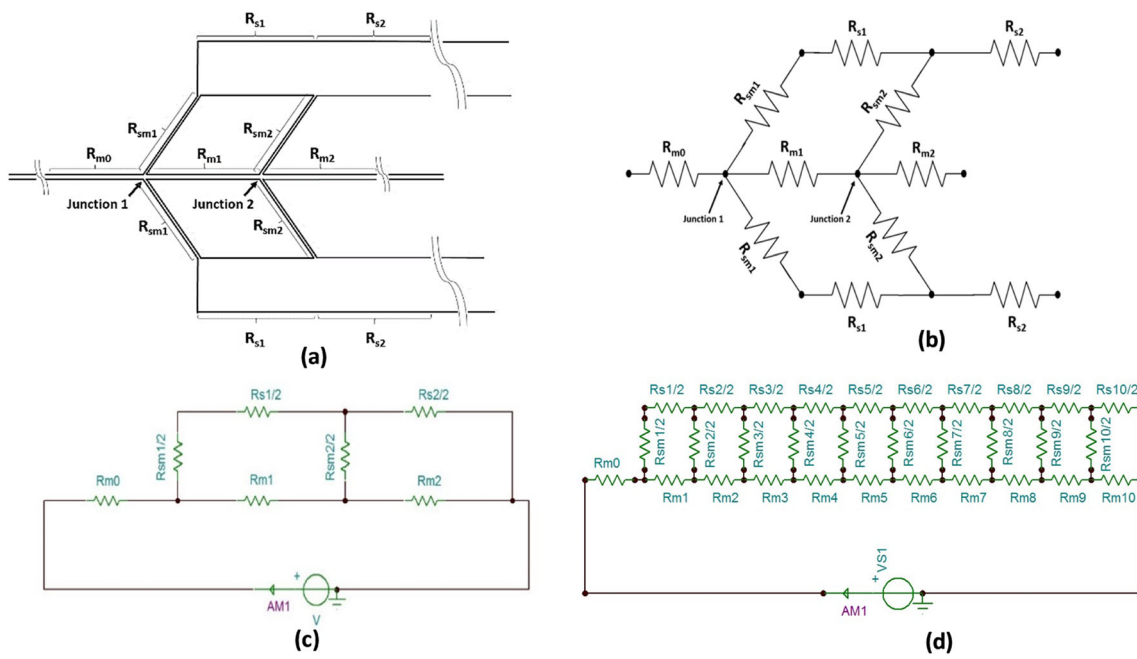


Fig. 2 Schematic of **a** a part of the fluidic network with two junctions and **b** its equivalent electrical network and **c** the reduced circuit **d** entire reduced circuit modelled in TINA-TI

The above equation can be presented in matrix form as follows,

$$\begin{pmatrix} R_{m1} & \left(-R_{sm1} \frac{R_{s1}}{2} - R_{m1}\right) & \frac{R_{sm1}}{2} \\ R_{m2} & \frac{R_{sm2}}{2} & \left(-\frac{R_{sm2}}{2} \frac{R_{s2}}{2} - R_{m2}\right) \\ (R_0 + R_{m1} + R_{m2}) & -R_{m1} & -R_{m2} \end{pmatrix} \begin{pmatrix} I_2 \\ I_3 \\ I_{1,2} \end{pmatrix} = \begin{pmatrix} 0 \\ 0 \\ V_{1,2} \end{pmatrix} \tag{5}$$

We can generalize the above matrix for the entire microchannel network with n number of bifurcations to obtain,

$$\begin{pmatrix} \lambda_1 & A_1 & \eta_1 & 0 & 0 & 0 & 0 & 0 & 0 & 0 \\ \lambda_2 & \eta_2 & A_2 & \eta_2 & 0 & 0 & 0 & 0 & 0 & 0 \\ \lambda_3 & 0 & \eta_3 & A_3 & \eta_3 & 0 & 0 & 0 & 0 & 0 \\ \dots & 0 & 0 & \eta_4 & A_4 & \eta_4 & 0 & 0 & 0 & 0 \\ \dots & 0 & 0 & 0 & \dots & \dots & 0 & 0 & 0 & 0 \\ \dots & 0 & 0 & 0 & 0 & \dots & 0 & 0 & 0 & 0 \\ \dots & 0 & 0 & 0 & 0 & 0 & \dots & 0 & 0 & 0 \\ \lambda_{n-1} & 0 & 0 & 0 & 0 & 0 & 0 & \eta_{n-1} & A_{n-1} & \eta_{n-1} \\ \lambda_n & 0 & 0 & 0 & 0 & 0 & 0 & 0 & \eta_n & A_n \\ \lambda^* & -\lambda_1 & -\lambda_2 & \dots & \dots & \dots & \dots & \dots & -\lambda_n & \dots \end{pmatrix} \begin{pmatrix} I_2 \\ I_3 \\ I_4 \\ \dots \\ \dots \\ \dots \\ \dots \\ I_{n+1} \\ I_{1,n} \end{pmatrix} = \begin{pmatrix} 0 \\ 0 \\ 0 \\ \dots \\ \dots \\ \dots \\ \dots \\ 0 \\ 0 \\ V_{1,n} \end{pmatrix} \tag{6}$$

Where $\lambda_i = R_{m,i}$ and $\eta_i = 0.5R_{smi}$ with $i=1, n, A_i = -(0.5R_{si} + \lambda_i + 2\eta_i)$, with $i=1, n-1$ and $A_n = -(0.5R_{sn} + \lambda_n + \eta_n)$, $\lambda^* = R_0 + \sum_1^n \lambda_i$. The above matrix is solved using MATLAB to determine flow rates (i.e., I_i with $i=1, n+1$) in each branch of the microchannel network. Additionally, the flow rates in each branch of the equivalent electrical circuit were also calculated by modelling the electrical circuit using TINA-TI software (Texas Instruments, USA), a SPICE based Analog Simulation program, as shown in Fig. 2d. First, the

above model is used to determine flow rates in all channels and at the cell and plasma outlets by considering water as the working fluid. Further, the flow rate ratios at each junction are calculated which is used for calculating the particle concentration after each junction (Xue et al. 2012), which affects their viscosity. Thus, viscosity varies along the main channel after each bifurcation. Assuming diluted blood as Newtonian fluid at higher shear rates ($>576 \text{ s}^{-1}$) and higher dilutions ($>50\times$) (Nivedita and Papautsky 2013; Tripathi et al. 2013; Xiangdong et al. 2007) and 100 % purification efficiency at every bifurcation, the plasma recovery is predicted and compared with that obtained from experiments. The particle concentration H_n (% Haematocrit) after n bifurcations was derived as (Xue et al. 2012).

$$H_n = H_0 \prod_{j=1}^n \left(1 + \frac{1}{R_j}\right) \tag{7}$$

Where R_j is the flow rate ratio at j^{th} bifurcation. The Eq. (7) is used to determine the haematocrit after every bifurcation. The relative viscosities for these haematocrit are calculated using Eqs (8–10) as (Pries et al. 1992),

$$\eta_{rel} = 1 + (\eta_{rel,0.45} - 1) \frac{(1-H)^{C-1}}{(1-0.45)^{C-1}} \tag{8}$$

$$\eta_{rel,0.45} = 220 \cdot e^{-1.3D} + 3.2 - 2.44 \cdot e^{-0.06 \cdot D^{0.645}} \tag{9}$$

$$C = (0.8 + e^{-0.075D}) \left(-1 + \frac{1}{1 + 10^{-11} \cdot D^{12}}\right) + \left(\frac{1}{1 + 10^{-11} \cdot D^{12}}\right) \tag{10}$$

Where η_{rel} and $\eta_{rel,0.45}$ are relative viscosities for haematocrit H and $H=0.45$ respectively, D is the diameter of the channel (in μm). The actual viscosity η_a was calculated from η_{rel} using a relation as follows.

$$\eta_a = \eta_{rel} \cdot \eta_s \quad (11)$$

Where η_s is the viscosity of the solvent. Here, phosphate buffered saline (PBS) was used for dilution of the blood sample ($\eta_s=0.00115\text{Pa}\cdot\text{s}$). The viscosity values calculated for different haematocrit in each channel section of the device were used in TINA-TI for calculating the flow rate at the plasma outlet. The results are later compared with that measured using experiments with diluted blood sample of haematocrit 0.4 %.

4 Numerical model

Numerical simulations (two-dimensional) were performed using volume of fluid (VOF) model in ANSYS-Fluent with mineral oil (density $\rho=840\text{ kg/m}^3$, dynamic viscosity $\mu=0.05\text{ Pa}\cdot\text{s}$) as the primary phase and water ($\rho=1000\text{ kg/m}^3$, $\mu=0.001003\text{ Pa}\cdot\text{s}$) as the secondary phase. Assuming flow to be incompressible, laminar and fully developed, the governing equations for mass, momentum and fluid fraction function are as follows:

$$\nabla \cdot u = 0 \quad (12)$$

$$\frac{\partial \rho u}{\partial t} + \nabla \cdot \rho u u = -\nabla P + \nabla \cdot (\mu(\nabla u + \nabla^T u)) + F_s \quad (13)$$

$$\frac{\partial F}{\partial t} + u \cdot \nabla F = 0 \quad (14)$$

Where u is the flow velocity, p is the pressure, ρ and μ are the density and viscosity of the fluid, respectively, F_s is the interfacial tension force which is added to the momentum equation as a source term and F is the volume fraction in a cell which has a value between 0 and 1. A detailed description of the VOF model is reported elsewhere (Sajeesh et al. 2014). Equations (12–14) are solved using appropriate boundary and initial conditions (for transient simulations with droplets). Velocity boundary condition is applied at the inlet and atmospheric pressure boundary condition is used at the outlets. Steady state simulations were performed with water as the working fluid to determine the location of the critical streamline (i.e., the streamline that separates the flow entering the side channels from that flowing along the main channel). The location and throat size of the constriction were also determined using the numerical simulations.

5 Experiments

5.1 Device fabrication

For the fabrication of the polydimethylsiloxane (PDMS) device, the optimised design of the device was made in AutoCAD LT 2008 which was printed on a flexi mask at 40000dpi (Fineline Imaging, USA). The silicon wafer (Semiconductor Technology and Application, Milpitas, USA) was cleaned using hydrofluoric acid (HF) solution (1:10) followed by deionised (DI) water and kept in oven (120 °C) for 2 min. To obtain a coating of thickness 50 μm , the negative photoresist SU8 2075 (MicroChem Corp, Newton, USA) was spun at 4000 rpm for 30s with an acceleration of 300 rpm/s. This was followed by soft baking at 65 °C for 3 min and hard baking at 95 °C for 6 min. The baked photoresist was then exposed to UV light (J500-IR/VISIBLE, OAI Mask alligner, CA, USA) through the mask for 6 s. Next, the wafer was then baked at 65 °C for 1 min and 95 °C for 5 min. The pattern was then developed by exposing it to SU8 developer and placed inside oven at 120 °C for 30 min. The PDMS monomer and the curing agent (Sylgard 184, Silicone Elastomer kit, Dow Corning, USA) at a ratio of 10:1 (by weight) was mixed and degassed. It was then poured onto the silicon master and was placed in a vacuum oven at 65 °C for 3 h for curing. The PDMS was peeled off from the master carefully and cut to size. Inlet and outlet holes were punched using 1.5 mm biopsy punch (Shoney scientific, Pondicherry, India). This PDMS layer was then bonded to a glass slide using an oxygen plasma bonder (Harrick Plasma, Brindley St., USA). Fluidic connections were provided to the device with the help of polyethylene tubings fitted with Luer stubs (Instech Laboratories, PA, USA). The photograph of the device and an optical image of the microchannel network are depicted in Fig. 3a and b, respectively.

5.2 Materials and methods

5.2.1 Droplets

It is reported in literature that RBCs can be assumed to behave like a liquid droplet wrapped in a membrane (Fung et al. 1993). So our initial experiments were performed using droplets. A droplet generator was introduced before the device inlet to generate discrete droplets which were separated from the continuous phase. Mineral oil (Acros Organics, Thermo Fisher Scientific, New Jersey, USA) with 5 % wt/wt Span 85 (Sigma Life Science) and DI water were used as the continuous and discrete phases, respectively. The flow rate of the discrete to continuous phase flow rate was adjusted to control the droplet size.

5.2.2 Microbeads

The bead sample was prepared by suspending 10 µm polystyrene beads (Sigma Aldrich, Bangalore, India) and 15 µm FluoSpheres (Life Technologies, USA) in 22 % wt/wt aqueous glycerol mixture to match the densities to prevent sedimentation (Sajeesh et al. 2014). Then, 5 % wt/wt Tween 80 (Sigma Aldrich, Bangalore, India) was also added as surfactant to ensure stability of the suspension throughout experiments. Three different concentrations of beads were prepared (1–3 µl/ml) and the mixture was sonicated for 3 min prior to use.

5.2.3 HL60 Cell line

HL60 (Human promyelocytic leukemia cells) cells purchased from NCCS (National Centre for Cell Sciences, Pune, India) were used as the cell model in our studies. These cells are predominantly a neutrophilic promyelocyte (precursor) which participate in the formation of certain types of blood cells. The cell size ranges from 10 to 20 µm. The cells were revived with Iscove's Modified Dulbecco's Medium (IMDM) (Himedia, India) containing 20 % FBS (Foetal Bovine Serum) (Gibco, Thermo Fisher Scientific). The cells were grown to 70–80 % confluency and seeded into suitable culture dishes of tissue culture grade for experiment. When confluence is attained, the cell culture medium was removed and the cells were washed twice with 1X PBS. Fresh medium containing 10 % serum was added to the cell pellet and re-suspended gently using micropipette. Cells were counted using a Improved Naeubaer Haemocytometer (Marienfeld, Germany) and a fixed number of cells were seeded into suitable dishes and maintained at cell culture growth conditions for experiments. The cells were transferred to 15 ml falcon tubes, with media

and centrifuged at 1700 rpm for 5 min. The supernatant was discarded and the pellet was re-suspended in 1.0 ml fresh media with Rhodamine (0.5 mg/ml) and incubated for 30 min. The cells were then pelleted down at 1700 rpm and the supernatant was discarded. The pellet was again re-suspended in 1.0 ml fresh media. With the help of Haemocytometer, samples of different concentrations i.e., 5×10^4 cells/ml, 1×10^5 cells/ml, 3×10^5 cells/ml, 5×10^5 cells/ml and 1×10^6 cells/ml were prepared and experimented.

5.2.4 Human blood sample

Samples of human blood from healthy donors were collected from hospital (Institute Hospital, IIT Madras) in vacutainers with 7.2 mg K2 Ethylene diamine tetraacetic acid (EDTA) (BD, New Jersey, USA). It was diluted to different haematocrits, namely 45 %, 20 %, 2 %, 0.04 %, 0.008 % with PBS.

5.2.5 Quantification of the separation process

(i) Purification Efficiency

Improved Neubauer Haemocytometer (Marienfeld-Superior, Germany) was used to count the number of beads or cells present in the samples at the device inlet and outlets. An aliquote of 10 µl of the sample was added to each of its chamber and viewed under microscope. The number of particles in a square of side 1.0 mm was counted on both the chambers and averaged to determine the number of particles present in 10 µl of sample. The % *Purification Efficiency* was calculated from the experiments as follows,

$$\% \text{Purification Efficiency } (\eta) = \left(1 - \frac{\text{Number of beads at plasma outlet}}{\text{Number of beads at cell outlet} + \text{Number of beads at plasma outlet}} \right) \times 100 \quad (15)$$

(ii) Plasma Recovery

The fluids obtained at the two outlets were collected

for a particular time interval and measured. The plasma recovery of the device was calculated as follows,

$$\% \text{Plasma recovery} = \frac{\text{Volume at Plasma Outlet}}{\text{Volume at Plasma Outlet} + \text{Volume at Cell Outlet}} \times 100 \quad (16)$$

(iii) Cell count and damage

In order to obtain information about the cell damage incurred during the process and to complement the purification efficiency measurements, flow cytometry studies were performed in a FACS Scan Instrument (Calibur, BD Biosciences). The inlet, cell outlet and

plasma outlet samples from experiments with HL60 and blood sample were appropriately diluted and tested. The Forward Scatter (FSC) is a measure of the size of the particle. Therefore a plot of FSC against the particle count in the inlet and outlet samples will provide an understanding of the number of cells of different size

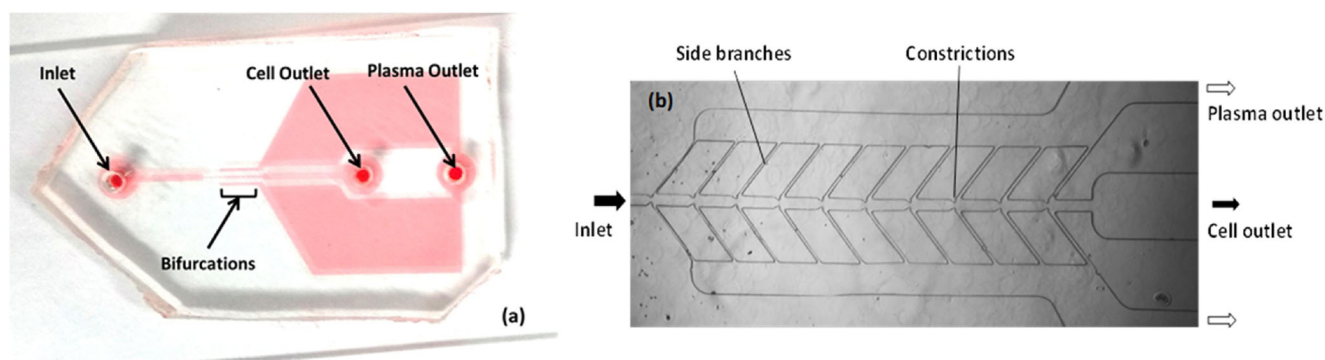


Fig. 3 **a** Photograph of the cell-plasma separation device filled with dye **b** Optical image of the microchannel network

groups present in the samples which can be used to validate cell separation. Also, comparison of FSC of outlet with the inlet sample will help in deduction of cell damage, if any, happening during the process.

(iv) Cell Viability

Cell viability after the separation process was assessed using Trypan Blue Test. Viable cells with intact cell membrane retain their original colour while damaged cells allow the entry of dye through the disrupted membrane to take up the colour of the dye. As part of the test, 10 μl of the sample and 10 μl of the Trypan blue dye were mixed. From the mixture, a 10 μl aliquot was taken to the haemocytometer chamber and viewed under the microscope. The number of non-viable cells were counted and the % cell viability was calculated as follows,

$$\% \text{ Cell Viability} = \frac{\text{Total no. of cells} - \text{No. of non-viable cells}}{\text{Total no. of cells}} \times 100 \quad (17)$$

5.3 Experimental setup

A schematic and a photograph of the experimental setup used for the cell-plasma separation experiments are shown in Fig. 4a and b, respectively. The sample fluids (containing droplets, particles or cells) were infused into the microfluidic device using a programmable syringe pump (Model 540060, TSE systems, Germany). The fluidic connection between the syringe pump and the device was established using polymer tubing (Instech Laboratories Inc, USA). After separation inside the device, the samples at the device outlets were collected in eppendorf tubes and used for further analysis. In order to reduce cell adhesion problem (i.e., sticking of cells with the channel wall), the microchannel device was initially filled with filtered 1 % Bovine Serum Albumin (BSA) in PBS buffer and left undisturbed for 30 min before cell samples were used. The motion of droplets, beads and cells were observed and

captured using an inverted microscope (Carl Zeiss Axiovert A1) coupled with a high-speed camera (FASTCAM SA3 model, Photron USA, Inc.) interfaced with PC via Photron Fastcam Viewer 3 software. The images of the samples were captured using reflecting type microscope (Carl Zeiss Axio Scope. A1) coupled with a CCD camera (ProgRes 391CF Cool, Jenoptik, Germany) interfaced with PC via ProgRes CapturePro v2.8.8 software.

6 Results and discussion

6.1 Design of the microchannel

The microchannel network (shown in Fig. 3b) was designed using the theoretical model and numerical simulations presented in section 3 and 4, respectively. It is reported in literature that the Fahraeus-Lindqvist effect is effective for a channel size in the range 40–300 μm (Fahraeus and Lindqvist 1931) and the effect is pronounced for a smaller channel size. Smaller channel sizes lead to higher chances of clogging and larger channel sizes weaken the effect and offer larger dead volume. Thus, in our design, the width of the main channel was selected to be 100 μm . In order to determine the width of the side channels, the effect of the side channel width on the total flow rate at the plasma outlet was studied, considering DI water as the working fluid ($\rho = 1000 \text{ kg/m}^3$, $\mu = 0.001003 \text{ Pa}\cdot\text{s}$). Figure 5 shows the variation of the ratio of the total flow rate at the plasma outlet to the inlet flow rate (i.e., Q_p/Q_i) with the ratio of the widths of the side channel to that of the main channel (i.e., w_s/w_m). It is observed that the total flow rate at the plasma outlet initially increases with increase in the width of the side channel and finally reaches a steady value. For $w_s/w_m > 0.25$, no significant change in the total flow rate at the plasma outlet is observed. So, the size of the side channels was selected to be 25 μm . The theoretical model was used to obtain the flow rate ratios Q_{m_i}/Q_{p_i} (i.e., ratio of flow rate in the main channel to that in the side channels) at each bifurcations and the results are presented in

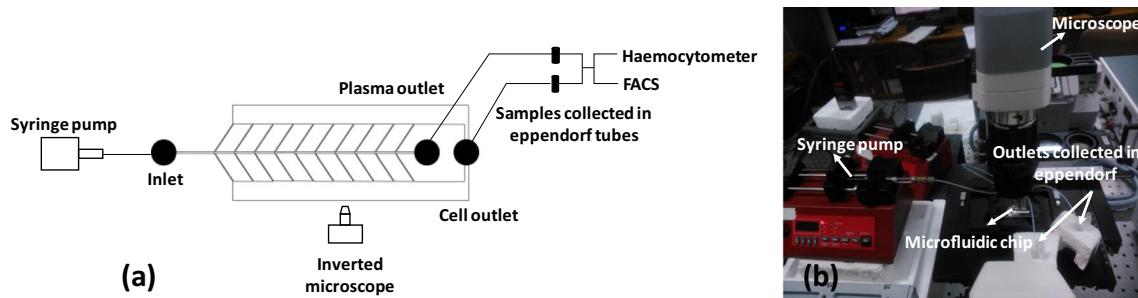


Fig. 4 **a** Schematic and **b** photograph of the experimental setup used for cell-plasma separation experiments

Fig. 6. As observed, the flow rate ratios increase at each bifurcation downstream which indicates that use of more number of bifurcations would not have considerable influence on the plasma extraction beyond a certain number of branches. Thus in our design the maximum number of side channels were limited to 10. A further increase in the number of side channels would result in much higher flow rate ratio which may cause cell damage (Tripathi et al. 2013) and excessive back pressure in the device. Then, variation of the total flow rate at the plasma outlet for different inlet flow rates was studied using experiments and compared with that predicted using the theoretical analysis and numerical simulations, as shown in Fig. 7. It was observed that the total flow rate at the plasma outlet increases linearly with the inlet flow rate, as expected and a very good match between the theoretical analysis/simulations and experiments was found (within 10 %). Similarly, the total flow rate at the plasma outlet for diluted blood (0.4 % haematocrit) was calculated using the Eqs. 7–11 and compared with that obtained using experiments as shown in Fig. 8. The match was found to be reasonable with a maximum error of 17 % which may be due to the approximations employed in the model.

Next, the variation in the distance of the critical streamline from the side wall with flow rate ratio (observed at different bifurcations) was studied for droplets of radius 5 μm and 10 μm (size comparable to that of RBCs 6–8 μm size and HL 60 cells 10–20 μm size), as shown in Fig. 9. In these VOF simulations, mineral oil ($\rho=840 \text{ Kg/m}^3$, $\mu=0.05 \text{ Pa.s}$) was taken as the primary phase and water ($\rho=1000 \text{ Kg/m}^3$, $\mu=0.001003 \text{ Pa.s}$) as the secondary phase. The interfacial tension was taken to be 24.4 mN/m. From literature (Narsimhan et al. 2013), it is known that the cell free layer thickness is equal to half the cell size. Therefore, in order to achieve 100 % purification efficiency, the critical streamline for a particular flow rate ratio must lie below T_s , where T_s is the total of the thickness of the cell free layer and the radius of the cell as shown in Fig. 10. It is observed that at all bifurcations except bifurcation 9, where the flow rate ratio is 6, the critical streamline width is much higher than T_s (e.g., at bifurcation 4, the critical streamline width of 21.5 μm is higher than T_s (10 μm) for a 10 μm droplet). Thus, a cell which is located close to the wall (which is possible particularly at high concentrations),

the cell would enter into the plasma channels. In order to take care of this, the device design was improved by introducing constrictions before each junctions. The constrictions are expected to direct cells flowing closer to the side walls towards the centre of the channel. The constrictions were designed such that the critical streamlines are located at a distance less than T_s (which is typically 2 μm for blood cells (Narsimhan et al. 2013)).

The variation of the location of the dividing streamline as a function of constriction width and length is given in Table 2. In this study, a bifurcation with a flow rate ratio of 3.6 was designed and a constriction was included at the junction and the critical stream width was verified. Initially, the length of the constriction was kept fixed at 40 μm while the constriction width was examined in the range 20–50 μm . Later, the width of the constriction was kept constant at 40 μm and the length was varied in the range 20–100 μm . It is observed that a constriction width <30 μm is required to provide the required drifting to cells to the desired location. However, such small dimensions of the constriction may lead to clogging issues. Also, at 20 μm , the simulation indicated a reverse flow from the plasma channel into the main channel and at 30 μm , the flow rate ratio was as high as 42.5 which could damage the cells. So, in our device a constriction width of 40 μm was used. The variation of constriction length showed negligible effect on the location of the streamlines. A constriction length

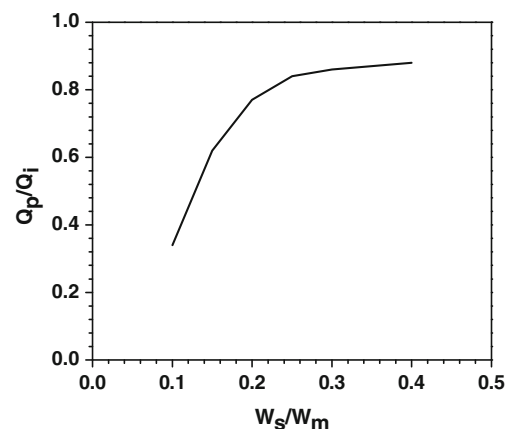


Fig. 5 Variation of the total plasma flow rate with width of the side channel

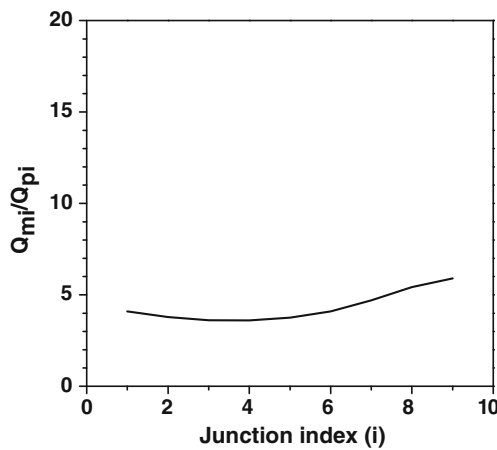


Fig. 6 Variation of flow rate ratio at different bifurcations

of 40 μm was found to have a safe non-detrimental flow rate ratio (<10). Further, the location of the constriction was decided by studying the effect of the distance of the constriction from the junction on the location of the dividing streamline using VOF method. There was not much variation in terms of the location of constriction observed by changing the distance of the constriction from the junction in the range 25 to 100 μm . However, the least critical stream width of 15 μm was observed when the constriction was placed right at the junction. A slanting constriction was observed to be the optimum geometry providing lesser critical stream width (12 μm) as compared to that in case of a straight geometry. Thus, the dimensions, location and the geometry of the constriction was optimized. Hence, a slanting constriction of 40 μm neck width, 40 μm length as shown in Fig. 11 was incorporated at every junction along the channel. The constrictions also give rise to the formation of recirculation zones (indicated in Fig. 11) at the wake of the constrictions where plasma is extracted into the side channels.

Next, VOF simulations were performed to show the dynamics of droplets of radius 5 μm at the junction with and

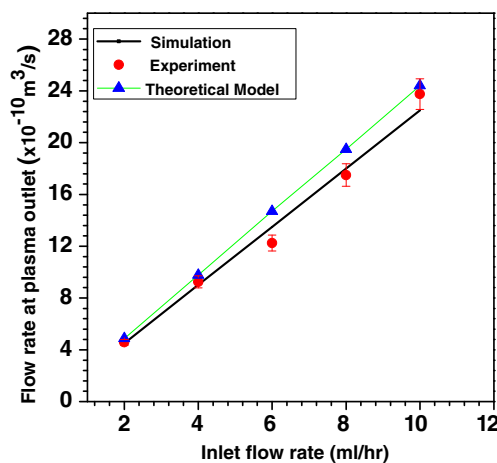


Fig. 7 Comparison of flow rate at plasma outlet obtained with DI water as working fluid

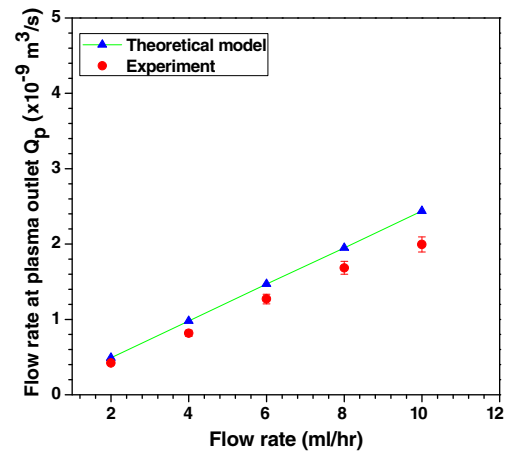


Fig. 8 Comparison of plasma flow rate with diluted blood sample as working fluid

without bifurcations. Figure 12 shows that without constrictions a droplet which is located closer to the wall (at a distance of 20 μm from the wall) moves into the side channel. By using a constriction before the junction, for the same flow rate ratio, the droplets get drifted towards centre of the channel and move along the main channel.

6.2 Experiments with droplets and microbeads

Before using the device for cell-plasma separation, experiments were performed with droplets and microbeads. DI water droplets were generated by using mineral oil as the continuous phase and DI water as the discrete phase. The flow rates of the continuous and discrete phases were 8 $\mu\text{l}/\text{min}$ and 0.25 $\mu\text{l}/\text{min}$, respectively to generate droplets of 20 μm size. These droplets are larger in size (as compared to the channel size) and thus always move towards the centre of the channel (Geislinger and Franke 2014). Because of the presence of droplets at the centre of the main channel and use of higher

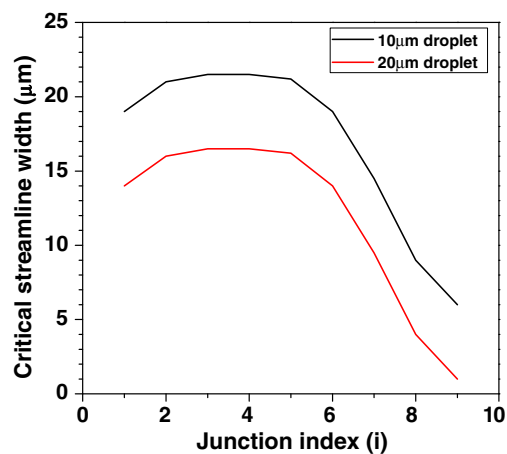


Fig. 9 Variation of critical streamline width at different bifurcations, droplet size 10 μm and 20 μm

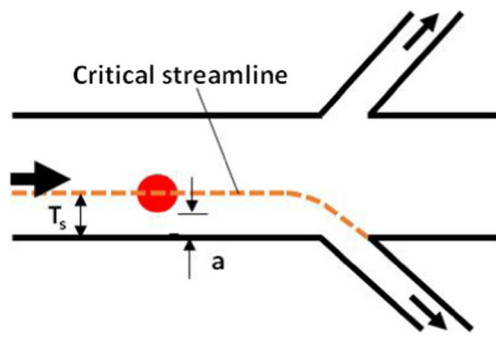


Fig. 10 Illustration of the critical streamline and the width T_s at a bifurcation

flow rate ratio (than the critical flow rate ratio) at each junction, the droplets continue to move along the main channel only and are collected at the cell outlet. A 100 % purification efficiency is observed in the case of droplets. Thus we could expect that RBCs which behave similar to droplets (Fung et al. 1993), if positioned at the centre of the channel, would follow bifurcation law and continue to flow along the main channel and get collected at the cell outlet to provide higher purification efficiency.

Experiments were performed using 10 μm polystyrene microbead samples suspended in 22 % glycerol solution at different concentrations in the range 1–3 $\mu\text{l/ml}$ at various flow rates between 2 and 10 ml/hr. For better visualization, images were taken for the movement of 15 μm red FluoSpheres. Figure 13a-b and c-d shows the movement of microbeads inside devices with and without constrictions, respectively. As observed in Fig. 13a, in a device without constrictions, the microbeads which are positioned at the centre of the channel continue to move along the main channel and get collected at the cell outlet. However, the microbeads that are located closer to the wall (at a distance below the critical streamline) enter into the side channels as seen in Fig. 13b. In a device with constrictions, depending on the initial location of the microbeads across the section, most of the beads are focused towards the centre of the channel at each junction and thus

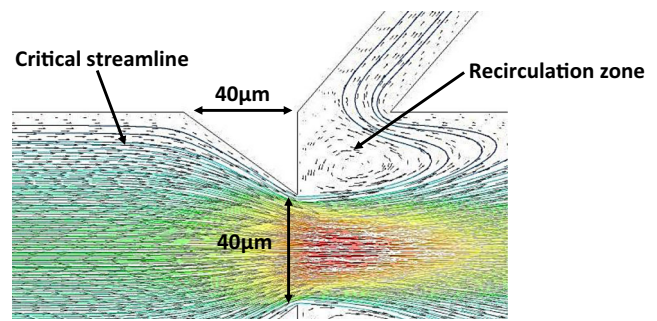


Fig. 11 Image showing the optimised constriction dimension with the streamlines showing the recirculation zone

move along the main channel, as shown in Fig. 13c. The beads which are in contact with the side walls still enter the side channels, as shown in Fig. 13d, and the throat of the constriction required to further avoid this is too small which may provide clogging problem. The concentrated microbead sample at the cell outlet was collected in an eppendorf tube and the microbead concentration was determined using haemocytometer. At a given flowrate, the concentration of microbeads at the device inlet and the cell outlet was used to calculate the purification efficiency using Eq 15. The effects of the inlet flow rate and microbead concentration on the purification efficiency in device without and with constriction was studied and the results are shown in Fig. 14a and b, respectively.

Figure 14a and b show that there is an increase in the efficiency when flow rate is increased upto 6 ml/hr beyond which a decrease is observed. The initial increase may be because the initially randomly distributed beads at low flow rates comes under the influence of higher wall and shear induced lift forces at increased flow rates. Spherical rigid particles are aligned at a thin annulus around 0.6 radii (0.6 R) from axis of the tube at higher flow rates (Geislinger and Franke 2014). This is the equilibrium position under the action of wall induced and shear induced lift forces. Here, highest purification efficiency is obtained at a flow rate of 6 ml/hr ($Re=15$). Further, it is known that the equilibrium position gets shifted

Table 2 Comparison of flow rate ratio and corresponding critical streamline position for different constriction width

Width of the constriction (μm)	Length of the constriction (μm)	Critical streamline width (μm)	Flow rate ratio
20	40	0	Reverse flow in the plasma channel
30		5	42.5
40		12	9.95
50		16	6.4
40	20	12	11.05
	40	12	9.95
	60	12.7	9.42
	80	13.2	9.2
	100	0	Reverse flow in the plasma channel

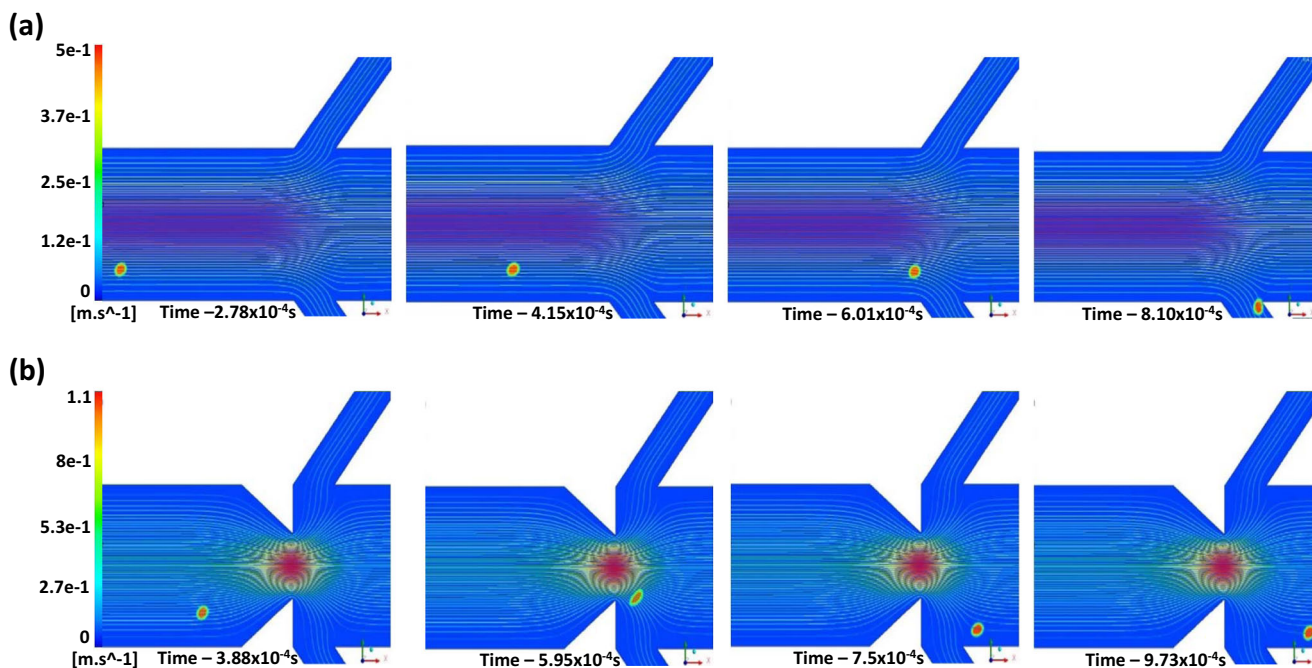


Fig. 12 VOF simulations showing the movement of droplet placed close to a wall in a channel with and without constriction. **a** movement of the droplet following the streamline into the side channel **b** constrictions help

in the movement of the droplet into the main channel by lowering the critical streamline width

towards wall at high Re (Geislinger and Franke 2014). This may be the reason for the drop in the efficiency beyond a flow rate of 6 ml/hr. Also, the purification efficiency decreases with increase in the particle concentration which may be due to the interaction between the beads to get focused below the critical streamlines and enter into the side channel. The purification efficiency obtained with the microbeads is smaller (~60 %) even when constrictions were employed which may be due to lesser force acting on the rigid spheres. The constrictions help in increasing the efficiency by pushing the critical streamline nearer to the wall. From Fig 14b, it can also be seen that constriction reduces the effect of concentration since more streamlines enter the main channel.

6.3 Experiments with HL60 cells

Experiments were performed with HL60 cells suspended in IMDM medium at different concentration in the range 5×10^4 – 1×10^6 cells/ml at various flow rates between 2 and 10 ml/hr. The size of the HL60 cells is measured to be $18 \pm 3 \mu\text{m}$. The cells are labeled with Rhodamine dye ($\lambda_{\text{ex}} = 541 \text{ nm}$, $\lambda_{\text{em}} = 565 \text{ nm}$) and observed with the help of a fluorescence attachment (HB0100 illumination system and FS14 filter, Carl Zeiss) with the inverted microscope which allows spectral width 510–560 nm. Figure 15a and b shows the movement of HL60 cells inside the device with and without constrictions, respectively. In device without constriction as seen Fig. 15a, similar to the microbeads, the cells which are positioned at the centre of the channel continue to move along the main channel

and get collected at the cell outlet. However, the cells that are located closer to the wall (at a distance below the critical streamline) enter into the side channels and thus affect the purification efficiency. In a device with constrictions, depending on the initial location of the cells across the section, most of the cells are focused towards the centre of the channel at each junction and thus move along the main channel, as

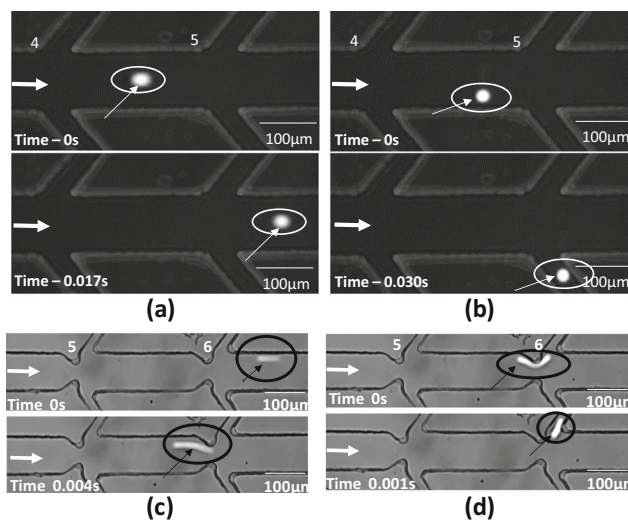
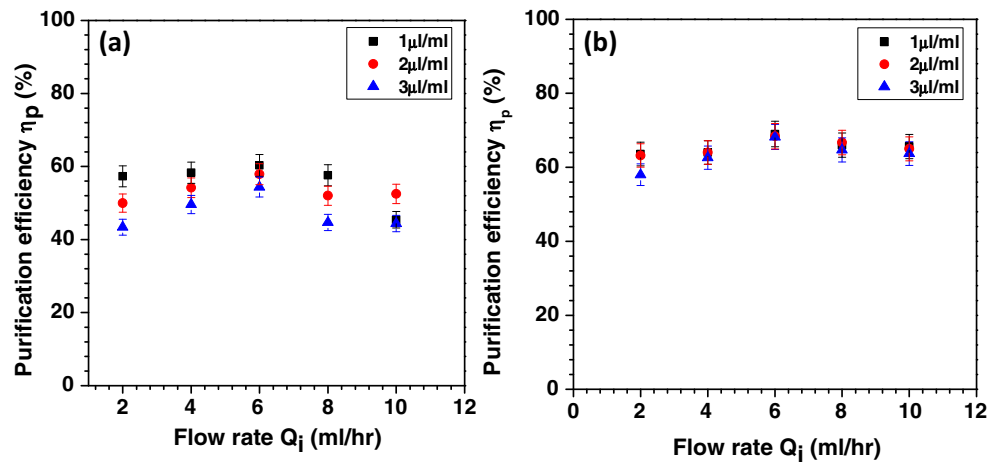


Fig. 13 Images showing the movement of beads in device **a** without constriction bead located closer to the centre moves along the main channel to cell outlet **b** without constriction bead very close to the wall moving into the side channel **c** with constrictions, the beads are focused towards the centre of the channel before a bifurcation, **d** with constrictions, beads sticking to the channel wall moving into the side channel

Fig. 14 Plots showing purification efficiency *versus* flow rate at three different concentrations **a** without constriction and **b** with constriction



shown in Fig. 15b. Some of the cells which are located closer to the side walls (within a distance of the order of the cell radius) their centre may get further close to the side walls due to cell deformation when cells are subjected to fluid shear. Such cells enter the side channels and affect the purification efficiency. The concentrated cells are collected at the cell outlet in an appendorf tube and their concentration was measured using haemocytometer which was used further to calculate the purification efficiency using Eq. 15. The effects of inlet flow rate, constriction and cell concentration on the purification efficiency was studied and the results are presented in Fig. 16. From Fig. 16a, it is observed that, at a cell concentration of 1×10^6 cells/ml, a maximum purification efficiency of $\sim 70\%$ is achieved with the device without constriction at a flow rate of 6.0 ml/hr. However, in case of a device with constrictions, the purification efficiency was improved to $\sim 99\%$. This is possibly due to the high shear stress zone

created locally as a result of the constriction which pushes the cells towards the channel centre (Faivre et al. 2006).

From Fig. 16b, it is observed that the purification efficiency using device with constriction is higher at lower cell concentrations and is highest at a flow rate of 6 ml/hr. This could be because of absence of cell-cell interaction at lower cell concentrations which may be adversely affecting the cell migration towards centre due to the wall-induced lift force. It is observed that a purification efficiency of $\sim 100\%$ is achieved for lower cell concentrations (i.e., within 5×10^4 cells/ml to 1×10^5 cells/ml). The purification efficiency increases with flow rate since the lift forces and the cell migration increases with flow rate (Geislinger and Franke 2014). After 6 ml/hr ($Re=28$), the efficiency decreases with flow rate. The cells being deformable take an elongated discoid shape and aligns parallel to the flow at higher flow rates which reduces the radius in the cross-stream direction and thus T_s decreases bringing it below

Fig. 15 Images showing experiment with HL60 cells **a** movement of HL60 cells located at different streamlines **b** the effect of constriction on focussing of the cells into the main channel

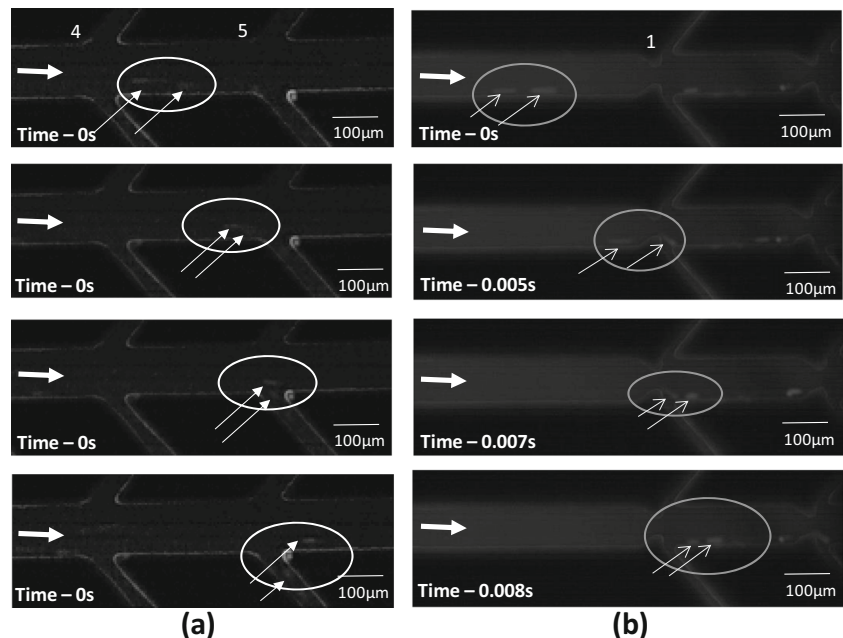
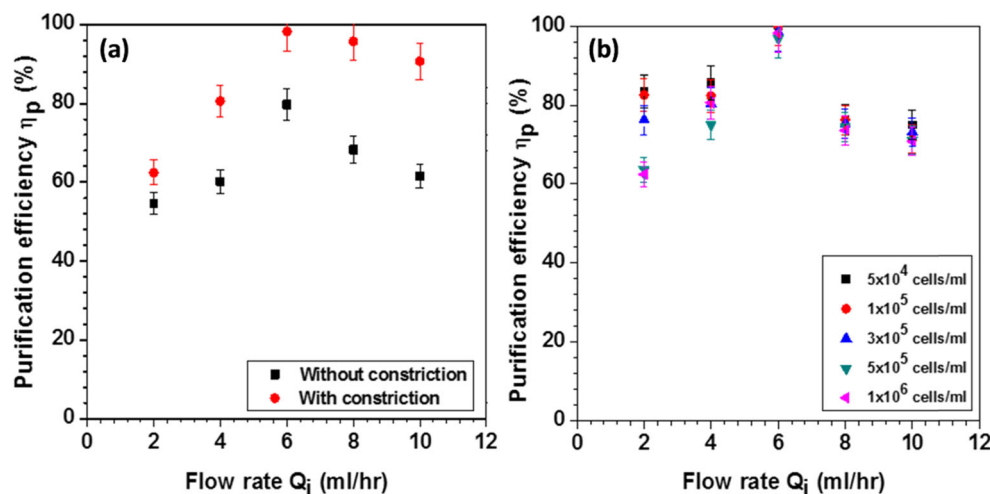


Fig. 16 **a** effect of constriction and flow rate on the purification efficiency, HL60 cells, concentration 1×10^6 cells/ml, **b** effect of HL60 cell concentration on purification efficiency at different flow rates in a device with constriction



the critical streamline. This may be the reason for the drop in efficiency. Another possible reason may be the high shear developing in the centre of the channel at high flow rates that increases the shear induced lift force thus breaks the equilibrium and pushes the cells towards the wall. A comparison of the purification efficiency achieved with microbeads explains the influence of deformability in the Fahraeus phenomenon which agrees with literature (Faivre et al. 2006; Tripathi et al. 2013; Narsimhan et al. 2013; Geislinger and Franke 2014). The purification efficiency was further validated using FACS. A cell sample at concentration 1×10^6 cells/ml is used at the device inlet at an inlet flow rate of 6.0 ml/hr and at the device outlets the cell and cell-free medium samples are collected separately. The separated cells as well as the cell-free medium are further diluted six-times to bring the total number of events in the sample below the maximum number of events set in the FACS instrument. A plot of FSC vs. Count was made after FACS measurement for the inlet sample, concentrated cell sample and cell-free medium as depicted in Fig. 17. It is observed that the number of events in the concentrated sample is very high indicating that most cells are collected at the cell outlet. Also, the number of events in the cell-free medium is extremely low which indicates that the device is capable of providing efficient cell separation and concentration.

6.4 Experiments with blood sample

Finally, experiments were performed with diluted blood samples (with PBS) at different dilution ratios in the range from whole blood to 1:5000 (haematocrit % in the range 45 %–0.008 %) at various flow rates between 2 and 10 ml/hr. Images showing separation of diluted blood sample into cells and plasma is depicted in Fig. 18a and b. In Fig. 18a, it can be seen that blood cell too close to the wall moves into the side channel, and in Fig. 18b, it is seen that the cells pushed towards nearer to the centre of channel than in the previous case

continue to move along the main channel whereas plasma is extracted through the side-channel. Figure 19a shows the effect of constriction and flow rate on purification efficiency and Fig. 19b shows the effect of dilution ratio on the purification efficiency. Similar to experiments with beads and cells, the purification efficiency was observed to be higher (>15 % at a haematocrit of 2 %), in case of a device with constriction as compared to a device without constriction. It can also be seen that the purification efficiency is maximum at 6.0 ml/hr as in the previous experiments. Study of the effect of dilution ratio in a device with constriction, presented in Fig. 19b, shows that a purification efficiency of 98 % is achieved at a dilution ratio of 1:5000 (haematocrit 0.008 %) and which reduces to 35 % for whole blood (haematocrit 45 %). A purification efficiency of 70 % and plasma recovery of 80 % is achieved with 2 % haematocrit (or 1:20 dilution) using this device, which is

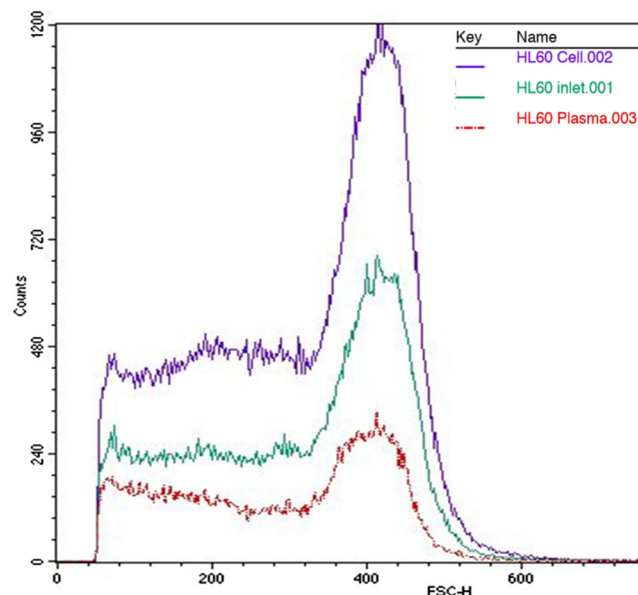
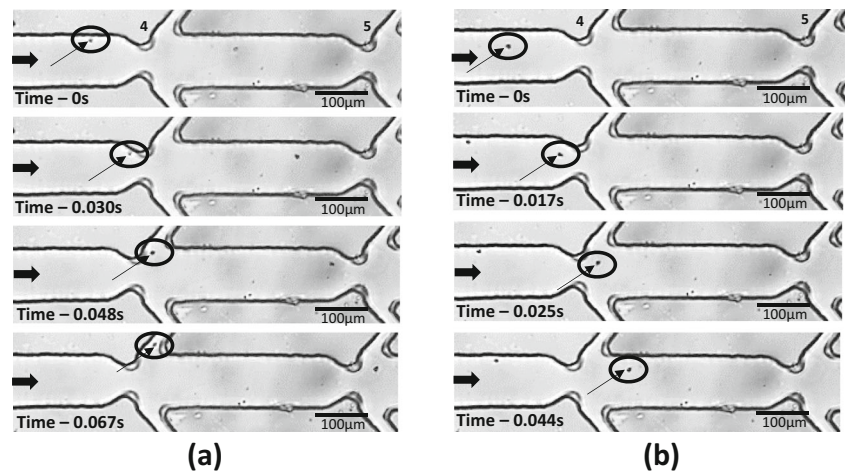


Fig. 17 Results of FACS studies with HL60 cells showing the number of events vs. forward scatter

Fig. 18 Images showing movement of blood cells inside a device with constrictions **a** movement of blood cell initially located near the wall into the side channels and **b** movement of cells near the centre into the main channel



better than the performance efficiency reported by Kersaudy-Kerhoas et al. (2010a) with a similar design. With all the dilution ratios, the efficiency is maximum at 6.0 ml/hr ($Re=20$). The trend in the purification efficiency is similar to HL60 cells due to the same reasons as mentioned in the previous section. Smaller size and higher deformability of RBC accounts for the lower efficiency as compared to the HL60 cells since the T_s is lower.

The effect of flow rate on plasma recovery is studied and it was found that plasma recovery is independent of the flow rate. The plasma recovery is found to be $>80\%$, which is higher as compared to what has been reported in literature. A comparison of performance of the proposed device with some of the cell-plasma separation devices (and the conventional centrifugation method) reported in literature is presented in Table 1. It is observed that our device has very good performance in terms of plasma recovery ($>80\%$) and purification efficiency ($\sim 70\%$ at haematocrit of 2%). FACS studies were carried out for a blood sample at dilution ratio of 1:1000 (Haematocrit $\sim 0.04\%$) and 1:20 (Haematocrit $\sim 2\%$). After separation, the cell and plasma samples are collected at the device outlets and further diluted to reduce the number of

events for measurements as in FACS study with HL60 cells. Figure 20 presents the plot of FSC vs. cell count. It is evident from the peaks in the plot that the cell concentration (RBCs and WBCs) has increased in the cell outlet and decreased in the plasma outlet, when compared with the inlet. While HL60 cells are $\sim 20\ \mu m$, RBC are only $\sim 8\ \mu m$. Since the lift forces depending on the cell size, in addition to the flow rate (Geislinger and Franke 2014), the design shows better efficiency with HL60 than with blood cells. The cell viability measurements using Trypan Blue test showed that the % cell viability (from Eq 17) is $>99\%$, which indicates that the device does not affect the cell viability and can be used for providing healthy blood cells for downstream analysis.

7 Conclusion

In this work, a microfluidic device for separating cells from a suspending fluid has been designed, fabricated and tested. A device with a series of bifurcations with dimensions optimized for flow rate ratios greater than the critical flow ratio, was designed and tested with droplets, polystyrene beads, HL60

Fig. 19 **a** Effect of constriction and flow rate on purification efficiency in experiments with blood sample of haematocrit 2% **b** Effect of dilution ratio on the purification efficiency at different flow rates in a device with constriction

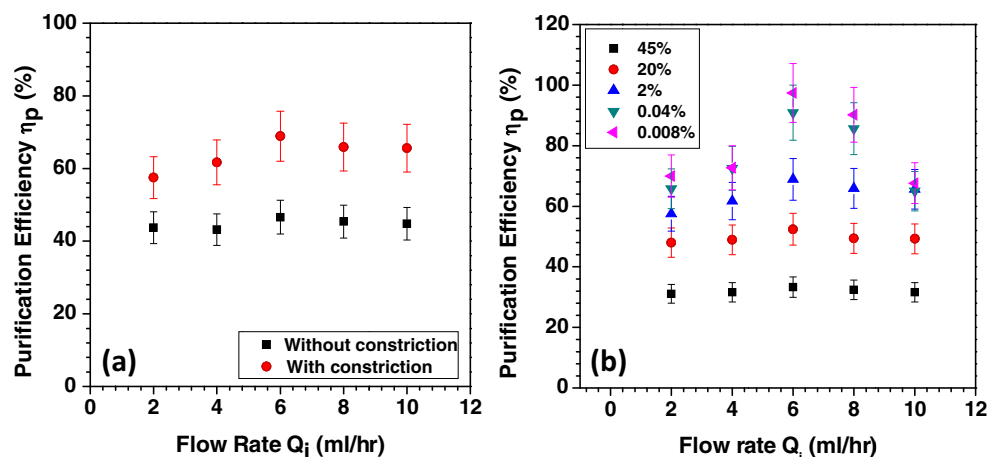
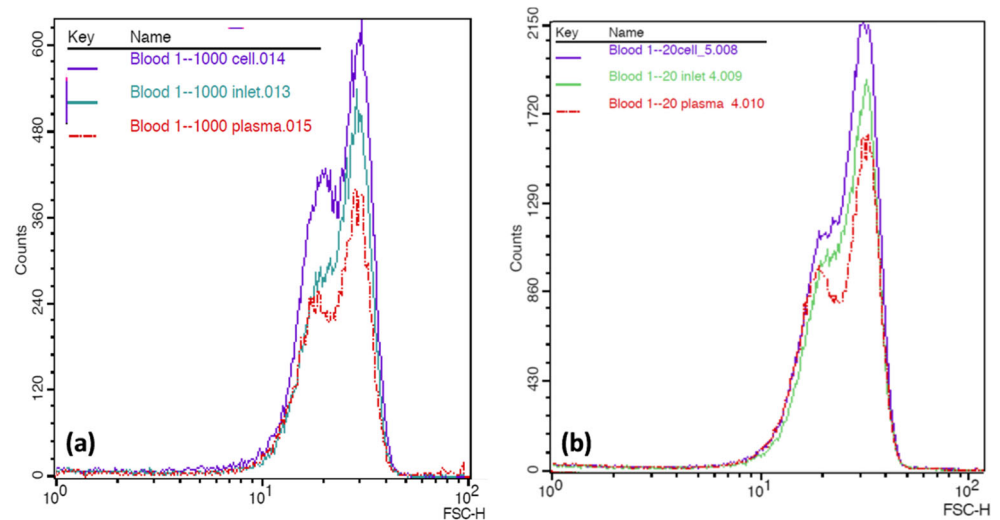


Fig. 20 FACS studies with blood sample of haematocrits **a** 0.04 %, **b** 2 %, showing number of events vs. the forward scatter, corresponding to the number of particles of different sizes present in the samples



and finally blood sample. Constrictions of neck width $40\ \mu\text{m}$ and length $40\ \mu\text{m}$ placed at the front of every bifurcation was found to increase the separation efficiency. The device with constrictions demonstrated a separation efficiency of $\sim 99\%$ with 1×10^6 HL60 cells/ml. It was capable of removing cells completely when lesser concentrations were tested at a flow rate of $6.0\ \text{ml/hr}$. A seven-fold cell concentration was obtained with HL60 cells. The difference between the separation of beads and cells implies the role of deformability and lift forces acting on the particles. When plasma separation from blood was investigated, it was found that considerable dilution (0.008% haematocrit) is required to reach $\sim 100\%$ separation. A purification efficiency of 70% and plasma recovery of 80% was observed for diluted ($1:20$ or 2% haematocrit) blood sample. The high plasma recovery of 80% makes the device stand out from previous works. The difference between the separation efficiencies achieved with HL60 and blood cells can be attributed to difference in the cell size. FACS studies on HL60 and blood sample further validates the working of the device and also showed that the device is more successful in separating HL60 cells from the sample. This is predicted in simulation that bigger particles will have its critical streamline closer to the wall, thus having better probability to flow into the main channel at every bifurcation. We believe that further improvements on the device to increase the flow rate ratios would improve the separation of RBCs at higher concentrations as well. Results from FACS and Trypan Blue test assure that the device is safe for cells (i.e., cells remain viable). Therefore, this device is a good candidate for blood plasma separator for integration with diagnostic device.

Acknowledgements The authors would like to thank Indian Institute of Technology Madras and the Department of Science & Technology (DST), India for providing the financial support for the project. We also acknowledge CNNP, IIT Madras for supporting the photolithography work. We thank Prof. Mukesh Doble and Ms. S. Manasi, Bio Engineering and Drug Design Lab, IIT Madras for the help with HL60 cell culture

used in this study. The authors also thank the Department of Biotechnology, IIT Madras for supporting with the FACS studies. Our special thanks to Interdisciplinary Program, IIT Madras which enabled this work.

References

- K. Aran, A. Fok, L.A. Sasso, N. Kamdar, Y. Guan, Q. Sun, A. Undar, J.D. Zahn, Microfiltration platform for continuous blood plasma protein extraction from whole blood during cardiac surgery. *Lab Chip* **11**, 2858–2868 (2011)
- A.A.S. Bhagat, H. Bow, H.W. Hou, S.J. Tan, J. Han, C.T. Lim, Microfluidics for cell separation. *Med. Biol. Eng. Comput.* **48**, 999–1014 (2010)
- P. Bhardwaj, P. Bagdi, A.K. Sen, Microfluidic device based on a microhydrocyclone for particle liquid separation. *Lab Chip* **11**, 4012–4021 (2011)
- C. Blattert, R. Jurischka, A. Schoth, P. Kerth, W. Menz, “Separation of blood cells and plasma in microchannel bend structures”. *Lab-on-a-Chip: Plat Dev Appl* **5591**, 143–151 (2004)
- S. Choi, J.K. Park, Continuous hydrophoretic separation and sizing of microparticles using slanted obstacles in a microchannel. *Lab Chip* **7**, 890–897 (2007)
- K.H. Chung, Y.H. Choi, J.H. Yang, C.W. Park, W.J. Kim, C.S. Ah, G.Y. Sung, Magnetically-actuated blood filter unit attachable to pre-made biochips. *Lab Chip* **12**(18), 3272–3276 (2012)
- T.A. Crowley, V. Pizziconi, Isolation of plasma from whole blood using planar microfilters for lab-on-a-chip applications. *Lab Chip* **5**, 922–929 (2005)
- J.A. Davis, D.W. Inglis, K.J. Morton, D.A. Lawrence, L.R. Huang, S.Y. Chou, J.C. Sturm, R.H. Austin, Deterministic hydrodynamics: taking blood apart. *PNAS* **103**, 14779–14784 (2006)
- I.K. Dimov, L. Basabe-Desmonts, J.L. Garcia-Cordero, B.M. Ross, A.J. Ricco, L.P. Lee, Stand-alone self-powered integrated microfluidic blood analysis system (SIMBAS). *Lab Chip* **11**, 845–850 (2011)
- V. Doyeux, T. Podgorski, S. Peponas, M. Ismail, G. Couplier, Spheres in the vicinity of a bifurcation: elucidating the zweifach–fung effect. *J. Fluid Mech* **674**, 359–388 (2011)
- R. Fahraeus and T. Lindqvist, “The viscosity of the blood in narrow capillary tubes”. *Am. J. Physiol.* **96**, 562–568 (1931)
- M. Faivre, M. Abkarian, K. Bickraj, H.A. Stone, Geometrical focusing of cells in a microfluidic device: an approach to separate blood plasma. *Biorheology* **43**, 147–159 (2006)

- R. Fan, O. Vermesh, A. Srivastava, B.K.H. Yen, L. Qin, H. Ahmad, G.A. Kwong, C. Liu, J. Gould, L. Hood, J.R. Heath, Integrated barcode chips for rapid, multiplexed analysis of proteins in microliter quantities of blood. *Nat. Biotechnol.* **26**(12), 1373–1378 (2008)
- Y. C. Fung, *Biomechanics: Mechanical Properties of Living Tissues*, Springer, 1993.
- E.P. Furlani, Magnetophoretic separation of blood cells at the microscale. *J. Phys. D. Appl. Phys.* **40**, 1313–1319 (2007)
- T.M. Geislinger, T. Franke, Hydrodynamic lift of vesicles and red blood cells in flow—from fähræus & lindqvist to microfluidic cell sorting. *Adv Colloid Interface Sci.* **208**, 161–176 (2014)
- D.R. Gossett, W.M. Weaver, A.J. Mach, S.C. Hur, H.T.K. Tse, W. Lee, H. Amini, D. Di Carlo, Label-free cell separation and sorting in microfluidic systems. *Anal. Bioanal. Chem.* **397**, 3249–3267 (2010)
- S. Haerberle, T. Brenner, R. Zengerle, J. Ducre'e, "Centrifugal extraction of plasma from whole blood on a rotating disk". *Lab Chip* **6**, 776–781 (2006)
- A. Homsy, P.D. van der Wal, W. Doll, R. Schaller, S. Korsatko, M. Ratzer, M. Ellmerer, T.R. Pieber, A. Nicol, N.F. de Rooij, "Development and validation of a low cost blood filtration element separating plasma from undiluted whole blood,". *Biomicrofluidics* **6**, 012804–1–9 (2012)
- H.W. Hou, A.A.S. Bhagat, W.C. Lee, S. Huang, J. Han, C.T. Lim, "Microfluidic devices for blood fractionation". *Micro Mach.* **2**, 319–343 (2011)
- R.D. Jaggi, R.S. Carlo, S. Effenhauser, Microfluidic depletion of red blood cells from whole blood in high-aspect-ratio microchannels. *Microfluid. Nanofluid.* **3**, 47–53 (2007)
- H. Jiang, X. Weng, C. H. Chon, X. Wu and D. Li, "A microfluidic chip for blood plasma separation using electro-osmotic flow control," *J. Micromech. Microeng.*, vol. 21, pp. 085019-1-8, 2011
- M. Kersaudy-Kerhoas, E. Sollier, Micro-scale blood plasma separation: from acoustophoresis to egg-beaters. *Lab Chip* **13**, 3323–3346 (2013)
- M. Kersaudy-Kerhoas, R. Dhariwal, M.P.Y. Desmulliez, Recent advances in microparticle continuous separation. *IET Nanobiotechnol.* **2**(1), 1–13 (2008)
- M. Kersaudy-Kerhoas, R. Dhariwal, M.P.Y. Desmulliez, L. Jouvet, Hydrodynamic blood plasma separation in microfluidic channels. *Microfluid. Nanofluid.* **8**, 105–114 (2010a)
- M. Kersaudy-Kerhoas, D.M. Kavanagh, R.S. Dhariwal, C.J. Campbell, M.P.Y. Desmulliez, Validation of a blood plasma separation system by biomarker detection. *Lab Chip* **10**, 1587–1595 (2010b)
- A. Lenshof, T. Laurell, Continuous separation of cells and particles in microfluidic systems. *Chem. Soc. Rev.* **39**, 1203–1217 (2010)
- A. Lenshof, A. Ahmad-Tajudin, K. Järås, A. Swärd-Nilsson, L. Åberg, G. Marko-Varga, J. Malm, H. Lilja, T. Laurell, "Acoustic whole blood plasmapheresis chip for prostate specific antigen microarray diagnostics". *Anal. Chem.* **81**, 6030–6037 (2009)
- C. Li, C. Liu, Z. Xu, J. Li, Extraction of plasma from whole blood using a deposited microbead plug (DMBP) in a capillary-driven microfluidic device. *Biomed. Microdevices* **14**, 565–572 (2012)
- S. Liao, C. Chang, H. Chang, "A capillary dielectrophoretic chip for real-time blood cell separation from a drop of whole blood". *Biomicrofluidics* **7**, 024110–1–9 (2013)
- A.J. Mach, D. Di Carlo, Continuous scalable blood filtration device using inertial microfluidics. *Biotechnol. Bioeng.* **107**(2), 302–311 (2010)
- J. Moorthy, D.J. Beebe, *In situ* fabricated porous filters for microsystems. *Lab Chip* **3**, 62–66 (2003)
- Y. Nakashima, S. Hata, T. Yasuda, Blood plasma separation and extraction from a minute amount of blood using dielectrophoretic and capillary forces. *Sensors Actuators B Chem.* **145**, 561–569 (2010)
- J. Nam, H. Lim, C. Kim, J.Y. Kang, S. Shin, "Density-dependent separation of encapsulated cells in a microfluidic channel by using a standing surface acoustic wave". *Biomicrofluidics* **6**, 024120–1–10 (2012)
- V. Narsimhan, H. Zhao, E.S.G. Shaqfeh, Coarse-grained theory to predict the concentration distribution of red blood cells in wall-bounded couette flow at zero Reynolds number. *Phys. Fluids* **25**, 1–10 (2013)
- N. Nivedita, I. Papautsky, "Continuous separation of blood cells in spiral microfluidic devices". *Biomicrofluidics* **7**, 054101–1–14 (2013)
- N. Pamme, Continuous flow separations in microfluidic devices. *Lab Chip* **7**, 1644–1659 (2007)
- A. Prabhakar, B.V. Kumar, S. Tripathi, A. Agrawal, "A novel, compact and efficient microchannel arrangement with multiple hydrodynamic effects for blood plasma separation,". *Microfluid. Nanofluid.* (2015). doi:10.1007/s10404-014-1488-6
- A.R. Pries, D. Neuhaus, P. Gaetgens, "Blood viscosity in tube flow: dependence on diameter and haematocrit,". *Am. J. Physiol.* **263**(6Pt2), H1770–1778 (1992)
- P. Sajeesh, A.K. Sen, Particle separation and sorting in microfluidic devices: a review. *Microfluid. Nanofluid.* **17**, 1–52 (2014)
- P. Sajeesh, M. Doble and A. K. Sen, "Hydrodynamic resistance and mobility of deformable objects in microfluidic channels," *Biomicrofluidics*, vol. 8, no. 5, 2014.
- A.K. Sen, T. Harvey, J. Clausen, T. Cox, "A microsystem for extraction, capture and detection of E-Coli O157:H7". *Biomedical Microdevices* **13**, 705–715 (2011)
- M. Sun, Z.S. Khan, S.A. Vanapalli, Blood plasma separation in a long two-phase plug flowing through disposable tubing. *Lab Chip* **12**, 5225–5230 (2012)
- M. Toner, D. Irimia, Blood-on-a-chip. *Annu. Rev. Biomed. Eng.* **7**, 77–103 (2005)
- S. Tripathi, A. Prabhakar, N. Kumar, S.G. Singh, A. Agrawal, "Blood plasma separation in elevated dimension T-shaped microchannel". *Biomed. Microdevices* **15**(3), 415–425 (2013)
- S. Tripathi, Y.V. Bala Varun Kumar, P. Amit, S.S. Joshi, A. Amit, Performance study of microfluidic devices for blood plasma separation—a designer's perspective. *J. Micromech. Microeng.* **25**, 084004 (2015a) (**15 pp**)
- S. Tripathi, Y.V.B.V. Kumar, A. Prabhakar, S.S. Joshi, A. Agrawal, Passive blood plasma separation at the microscale: a review of design principles and microdevices. *J. Micromech. Microeng.* **25**, 083001 (2015b) (**24 pp**)
- V. VanDelinder, A. Groisman, Separation of plasma from whole human blood in a continuous cross-flow in a molded microfluidic device. *Anal. Chem.* **76**(11), 3765–3771 (2006)
- A.P. Wong, M. Gupta, S.S. Shevkopylas, G.M. Whitesides, Egg beater as centrifuge: isolating human blood plasma from whole blood in resource-poor settings. *Lab Chip* **8**, 2032–2037 (2008)
- Xiangdong Xue, MayurK Patel and Chris Bailey, Challenges in Modelling Biofluids in Microchannels", 2nd Electronics Systemintegration Technology Conference Greenwich, UK. 2007.
- C. Xu, Y. Wang, M. Cao, Z. Lu, Dielectrophoresis of human red cells in microchips. *Electrophoresis* **20**, 1829–1831 (1999)
- X. Xue, M.K. Patel, M. Kersaudy-Kerhoas, M.P.Y. Desmulliez, C. Bailey, D. Topham, Analysis of fluid separation in microfluidic T-channels. *Appl. Math. Model.* **36**(2), 743–755 (2012)
- M. Yamada, M. Nakashima, M. Seki, Pinched flow fractionation: continuous size separation of particles utilizing a laminar flow profile in a pinched microchannel. *Anal. Chem.* **76**, 5465–5471 (2004)
- S. Yang, A. Undar, J.D. Zahn, A microfluidic device for continuous, real time blood plasma separation. *Lab Chip* **6**, 871–880 (2006)
- L.Y. Yeo, J.R. Friend, D.R. Arifin, "Electric tempest in a teacup: the tea leaf analogy to microfluidic blood plasma separation". *Phys. Lett.* **89**, 103516–1–3 (2006)
- Y. S. Yoon, S. Yang, Y. Moon and K. C. Kim, presented in part at MicroTas 2006, Tokyo, Japan, 2006
- X.B. Zhang, Z.Q. Wu, K. Wang, J. Zhu, J.J. Xu, X.H. Xia, H.Y. Chen, Gravitational sedimentation induced blood delamination for continuous plasma separation on a microfluidics chip. *Anal. Chem.* **84**, 3780–3786 (2012)
- R. Zhong, N. Wu, Y. Liub, Microfluidic human blood plasma separation for Lab on chip based heavy metal detection. *ECS Trans.* **41**(38), 11–16 (2012)